Improved method for isochromatic demodulation by RGB calibration

Juan Antonio Quiroga, Ángel García-Botella, and José Antonio Gómez-Pedrero

The red–blue–green (RGB) calibration technique consists in constructing an *a priori* calibration table of the isochromatic retardation versus the triplet of RGB values obtained with a RGB CCD camera. In this way a lookup table (LUT) is built in which the entry is the corresponding RGB triplet and the output is the given retardation. This calibration (a radiometric quantity) depends on the geometric and chromatic parameters of the setup. Once the calibration is performed, the isochromatic retardation at a given point of the sample is computed as the one that minimizes the Euclidean distance between the measured RGB triplet and the triplets stored in the LUT. We present an enhanced RGB calibration algorithm for isochromatic fringe pattern demodulation. We have improved the standard demodulation algorithm used in RGB calibration by changing the Euclidean cost function to a regularized one in which the fidelity term corresponds to the Euclidean distance between RGB triplets; the regularizing term forces piecewise continuity for the isochromatic retardation. Additionally we have implemented a selective search in the RGB calibration LUT. We have tested the algorithm with simulated as well as real photoelastic data with good results. © 2002 Optical Society of America

OCIS codes: 100.2000, 120.5630, 120.4290.

1. Introduction

Photoelasticity is a well-established technique for stress analysis. Although it is the only optical technique for measurement of stress, it fell into disuse with the advent of finite element methods and modern computing facilities. Recently, because of the application of new fringe-pattern analysis algorithms, this classical technique has received renewed interest for industrial as well as research applications.

As is well known, when a body is subjected to a three-dimensional (3D) state of stress, the generated stress at each point of the body can be represented as a symmetric second-order tensor. This tensor can therefore be diagonalized, with the eigenvalues being the principal stresses and the eigenvectors the principal directions. In two-dimensional (2D) samples under a 2D state of stress, two principal stresses are enough to describe the problem. The molecular deformations induced by the state of stress generate an inhomogeneous anisotropy that is the origin of the photoelastic phenomena. Although in this paper we are dealing with 2D photoelasticity, it should be noted that 3D states of stress in transparent bodies can also be studied by this technique.[1]

For the analysis of photoelastic fringe patterns, various techniques have been applied, such as phase shifting,[2] Fourier transforms,[3] spectral content analysis,[4] tricolor image analysis,[5] red–blue–green (RGB) calibration,[6,7] load stepping,[8] and regularization techniques.[9,10] One of the objectives in these techniques is the use of the smallest possible number of images.

In the case of isochromatic fringe patterns, tricolor, spectral content analysis, regularization, Fourier transform, and RGB calibration techniques need only one image, which is obviously the smallest possible number. This is an interesting feature when temporally varying phenomena are to be analyzed, such as in photoviscoelasticity or flow analysis.

The RGB calibration technique[6] consists in constructing an *a priori* calibration of the isochromatic phase versus the triplet of RGB values obtained with a RGB CCD camera. Within this framework the phase of the isochromatic fringe pattern is denoted isochromatic retardation or simply retardation, a term more frequently used in photoelasticity. In this way a lookup table (LUT) is built in which the

The authors are with the Departamento de Óptica, Facultad de Ciencias Físicas, Universidad Complutense, Ciudad Universitaria s/n, 28040 Madrid, Spain. J. A. Quiroga's e-mail address is aq@fis.ucm.es.

Received 5 September 2001; revised manuscript received 4 February, 2002.

0003-6935/02/173461-08$15.00/0

© 2002 Optical Society of America

entry is the corresponding RGB triplet and the output is the given retardation. For example, in the case of a circular polariscope used in the circular dark-field configuration with a white-light illumination source, if we neglect possible error sources such as the miscalibration of the quarterwave plates, the obtained RGB values can be expressed as

$$R = \int \bar{r}(\lambda) S(\lambda) \sin^2\left(\frac{\Delta}{\lambda}\right) d\lambda,$$

$$G = \int \bar{g}(\lambda) S(\lambda) \sin^2\left(\frac{\Delta}{\lambda}\right) d\lambda,$$

$$B = \int \bar{b}(\lambda) S(\lambda) \sin^2\left(\frac{\Delta}{\lambda}\right) d\lambda. \quad (1)$$

Here $\bar{r}(\lambda)$, $\bar{g}(\lambda)$, and $\bar{b}(\lambda)$ denote the response of the CCD camera as functions of the wavelength λ; $S(\lambda)$ is a spectral function that includes the spectrum of the light source and the transmission spectrum of the sample and objective; and Δ is the retardation in nanometers given by $\Delta = \pi C(\sigma_1 - \sigma_2)d$, where C is the photoelastic constant of the material (in a more general case its dependence on λ should be considered), σ_1 and σ_2 are the two principal stresses, and d is the thickness of the sample. In this way stress differences $(\sigma_1 - \sigma_2)$ cause fringes in the in the R, G, and B components of a color image. The fringes for each image have different angular displacements for each color component. This permits inversion from a single RGB image with an extended range of stresses with no need for phase unwrapping. Having three components makes the inverse relation of the stress differences to the components unambiguous.

Equations (1) describe the relation between isochromatic retardation and the obtained RGB values, but this is only a particular case; RGB calibration techniques have also been applied to shape measurement[11] and thin-film thickness measurements,[12] for example. Figure 1 shows a typical RGB LUT, in which each of the three channels is represented as a 2D plot as a function of $\sigma_1 - \sigma_2$.

From Eqs. (1) it is clear that the RGB calibration depends on the geometric and chromatic parameters of the setup. As examples of geometric parameters we can include the numerical aperture of the camera and the separation between the camera and the polariscope bench. In contrast, the thickness of the sample, the transmission spectrum of the sample, the polariscope and the camera, and the emission spectrum of the light source can be considered chromatic parameters. We make this distinction because, as we discuss below, these two classes of parameters have different effects on the measured radiometric quantities (the RGB values) and therefore on the RGB LUT algorithm.

In the standard algorithm, once the calibration is performed, the isochromatic retardation at a given point of the sample is computed as the one that minimizes the Euclidean distance between the measured RGB triplets and the triplets stored in the RGB LUT. That is, if the RGB LUT is defined as a matrix with three columns and N rows, $[\hat{R}(\Delta_i), \hat{G}(\Delta_i), \hat{B}(\Delta_i)]$, $i = 1 \ldots N$, with being N the number of calibration samples and Δ_i the corresponding *a priori* known retardations, the retardation $\delta(\mathbf{r})$ at a given location $\mathbf{r} = (x, y)$ with RGB value $[R(\mathbf{r}), G(\mathbf{r}), B(\mathbf{r})]$ is computed as the value Δ_i that minimizes the local cost function

$$U(\mathbf{r}, \Delta_i) = [R(\mathbf{r}) - \hat{R}(\Delta_i)]^2 + [G(\mathbf{r}) - \hat{G}(\Delta_i)]^2 + [B(\mathbf{r}) - \hat{B}(\Delta_i)]^2. \quad (2)$$

Obviously, the range of the retardation to be demodulated, δ, must be within the RGB LUT range.

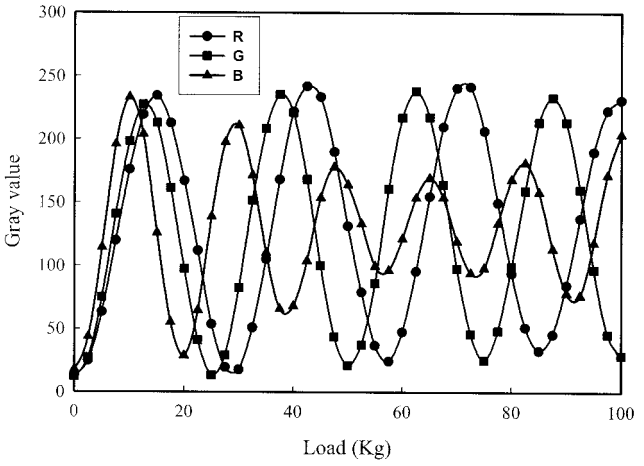

Fig. 1. Plot of the R, G, and B channels of a experimental RGB LUT. Points (symbols), experimental values; solid curves, interpolation.

The main advantages of the RGB calibration technique are that, once the calibration (implemented as a RGB LUT) is completed, the demodulation of an isochromatic pattern needs only one image and that this demodulation is direct in the sense that there is no need for further processing, such as phase unwrapping. In fact the output of this method is the continuous retardation over the whole image. The three-dimensional nature of the RGB curve arising from changing retardation is an alternative route toward demodulation of RGB images. In the standard procedure represented by Eqs. (1), as long as the RGB curve does not intersect itself within noise tolerances, an RGB value can be converted to stress differences.

However, in spite of the above advantages, there are some drawbacks of the method that must be taken into account. The first is that if the geometric or chromatic conditions under which the RGB LUT was determined were to change, the calibration would no longer be valid. The way a change in the measurement conditions affects the method depends on their the nature of the changes. If the chromatic parameters are modified, it is necessary to perform a new calibration; from Eqs. (1) it is clear that if $S(\lambda)$ changes then a new RGB LUT is generated as a function of Δ. Otherwise, if the change in the mea-

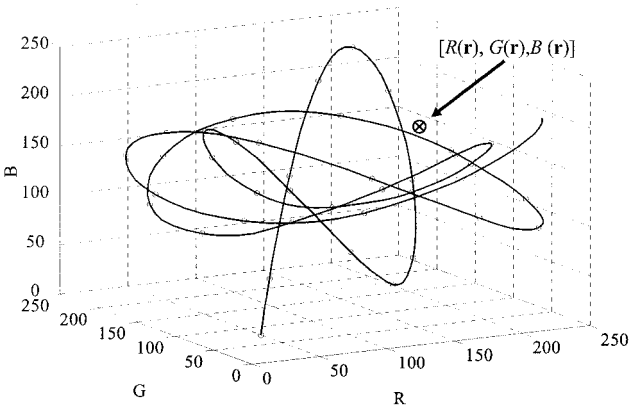

Fig. 2. 3D curve described in RGB color space for the RGB LUT depicted in Fig. 1. The points (Faint circles) were obtained experimentally, and the solid curve is the interpolation.

surement conditions affects only the geometric parameters (that is, introduces a multiplicative factor for the incident irradiances), one possibility is that chromatic coordinates r, g, b might be used instead of R, G, B values for the construction of the LUT (in this case denoted the rgb LUT). The chromatic coordinates are given by

$$r = \frac{R}{R+G+B},$$
$$g = \frac{G}{R+G+B},$$
$$b = \frac{B}{R+G+B}. \tag{3}$$

However, the noise amplification produced by the quotients of Eqs. (3) makes application of the standard calibration algorithm unreliable with the rgb LUT.

The second problem is the impulsive noise produced as a result of the geometrical structure of the RGB LUT considered as a 3D curve with parameter Δ. The RGB LUT 3D curve tends to form closed loops in the RGB space, so it can happen that the portion of the curve corresponding to retardation levels in the range of 10π rad can be very close to the portion corresponding to retardation values near 6π rad; thus the Euclidean distance, Eq. (2), is not sufficent to discriminate the actual branch to which the RGB triplet, obtained at the given location $\mathbf{r}$, corresponds; as a consequence impulsive noise with an amplitude of 4π rad, can appear surrounding of this location. This situation is represented in Fig. 2. In this figure the $[\hat{R}(\Delta_i), \hat{G}(\Delta_i), \hat{B}(\Delta_i)]$ curve was obtained experimentally for 40 measurements from fringe orders 0–4 (for $\lambda_{Na} = 589$ nm). As can be seen in Fig. 2, a given RGB triplet at location $\mathbf{r}$, $(R(\mathrm{r}), G(\mathrm{r}), B(\mathrm{r}))$, can be close to a branch crossing of the RGB LUT; because every branch corresponds to a different retardation, as explained above, impulsive noise can appear at location $\mathbf{r}$. For low fringe orders (up to 3), using different calibrations for dark and bright conditions of the circular polariscope and further filtering can alleviate this problem.[13] However, for higher fringe orders the impulsive noise increases, making application of the standard algorithm represented by Eq. (2) invalid.

In this paper we present a modified RGB calibration algorithm for isochromatic fringe pattern demodulation that overcomes the above-mentioned problems. First, we have changed the Euclidean cost function to a regularized one in which the fidelity term corresponds to the Euclidean distance between RGB triplets and the regularizing term forces piecewise continuity for the isochromatic retardation. Second, the implementation of a selective search in the RGB LUT reinforces the piecewise continuity imposed by the regularization term, and reducing the number of comparisons reduces the computing time. As a consequence of these modifications, application of the rgb LUT instead of the RGB LUT becomes reliable, making the RGB calibration algorithm more robust against variations in geometric parameters. The preliminary results of this method were outlined in Ref. 7, and in this paper the final technique is presented. First the measurement technique for the experimentally obtained RGB LUT is described, and its error level is estimated. Second, the roles of the geometric and the radiometric parameters are clarified, and the validity of a technique based on chromatic coordinates independent of geometric parameters is demonstrated. Third, an error analysis is performed, and conclusions about the best setup and illumination system are presented. Finally, the analysis of an alternative error-based method for stress demodulation from the RGB LUT is performed.

This paper is organized as follows: in Section 2 we present the theoretical foundations of the RGB calibration algorithm as well as numerical simulations; in Section 3 the results of the application of the algorithm to real experimental data are presented; finally, in Section 4 conclusions are given.

2. Improved RGB Calibration Algorithm

As we have discussed, we have changed the Euclidean cost function, Eq. (2), to a regularized version; in particular the version we propose is

$$\hat{U}(\mathbf{r}, \Delta_i) = [R(\mathbf{r}) - \hat{R}(\Delta_i)]^2 + [G(\mathbf{r}) - \hat{G}(\Delta_i)]^2 + [B(\mathbf{r}) - \hat{B}(\Delta_i)]^2 + \beta \sum_{\mathbf{s}} [\Delta_i - \delta(\mathbf{s})]^2 m(\mathbf{s}), \tag{4}$$

where β is the so-called regularization parameter, $\mathbf{s}$ denotes locations belonging to a defined neighborhood of site $\mathbf{r}$ (for example, its eight surrounding pixels), $m(\mathbf{s})$ is a mask that indicates whether the location $\mathbf{s}$ has already been processed, and $\delta(\mathbf{s})$ is the demodulated retardation at location $\mathbf{s}$. The first three terms on the right hand side reflect the closeness of the observations $(R(\mathbf{r}), G(\mathbf{r}), B(\mathbf{r}))$ to the RGB

LUT and together are called the fidelity term in regularization theory. The Fourth term is called the regularization term, and it incorporates the *a priori* knowledge that we have about the field to be recovered from the observations; in the case of Eq. (4), the regularization term imposes piecewise continuity on δ.

The demodulation procedure is as follows; for each site $\mathbf{r}$ of the RGB fringe pattern a one-dimensional array of length N is constructed according to Eq. (4). Then we look for the Δ_i at which $\hat{U}(\mathbf{r}, \Delta_i)$ is minimum; let us call this value Δ_{MIN}. Finally, we compute the retardation at position $\mathbf{r}$ as $\delta(\mathbf{r}) = \Delta_{\mathrm{MIN}}$. The role of the regularization term is to impose piecewise continuity on the demodulated phase field δ; the regularization parameter β controls the smoothness of the recovered phase. Typical values are in the range 1–10. At the starting point the processing mask is zero everywhere, so the minimization takes into account only the fidelity term. We start the demodulation at the location within the fringe pattern with the minimum value for the sum $R + G + B$, which in our case corresponds to low retardations.

With the procedure described above the demodulated retardation δ is discrete in the sense that the attainable values must be any of the N Δ_i retardations stored in the RGB LUT. Finer retardation values can be obtained if the RGB LUT is interpolated; typical interpolation factors are 10–20.

To test the procedure described above, we generated a RGB LUT with the $[\hat{R}(\Delta_i), \hat{G}(\Delta_i), B(\Delta_i)]$ values obtained with a linear retardation Δ_i used for the range of fringe orders 0–11.3 (for $\lambda_{\mathrm{Na}} = 589$ nm) and with Eqs. (1) for the spectrum of a discrete fluorescent lamp used in the real experiments, with square RGB CCD responses.

In Fig. 3 we show a plot corresponding to the RG-plane projection of the $[\hat{R}(\Delta_i), \hat{G}(\Delta_i), \hat{B}(\Delta_i)]$ values obtained for the simulated RGB LUT, superposed on the corresponding $(R(\mathbf{r}), G(\mathbf{r}), B(\mathbf{r}))$ values of a Gaussian retardation distribution corrupted with additive noise. For uncooled CCD cameras, electronic additive noise with a normal distribution is the most important source of noise; for this reason we have used it for the simulation. As can be observed, the effect of the noise is to widen the projection of the $(R(\mathbf{r}), G(\mathbf{r}), B(\mathbf{r}))$ curve.

In addition to the regularization term, we have implemented another technique to reinforce the reliability of the RGB calibration method. When one has to search for the Δ_{MIN} retardation, one possibility is to use the entire RGB LUT. In this case, even with the regularized cost function, Eq. (4), it is possible to make an error because of the complexity of the $[\hat{R}(\Delta_i), \hat{G}(\Delta_i), \hat{B}(\Delta_i)]$ curve for high fringe orders. To avoid this, we have implemented a selective search. In this case we do not use the entire RGB LUT; instead we use only a subset of $M < N$ $[\hat{R}(\Delta_i), \hat{G}(\Delta_i), \hat{B}(\Delta_i)]$ triplets, centered on the last retardation value obtained. In this way, as the algorithm progress spatially, the selective search moves the window that defines which part of the RGB LUT we are using for each location $\mathbf{r}$. As in the case of the regularized equation (4), the main assumption is the piecewise continuity of the retardation spatial distribution.

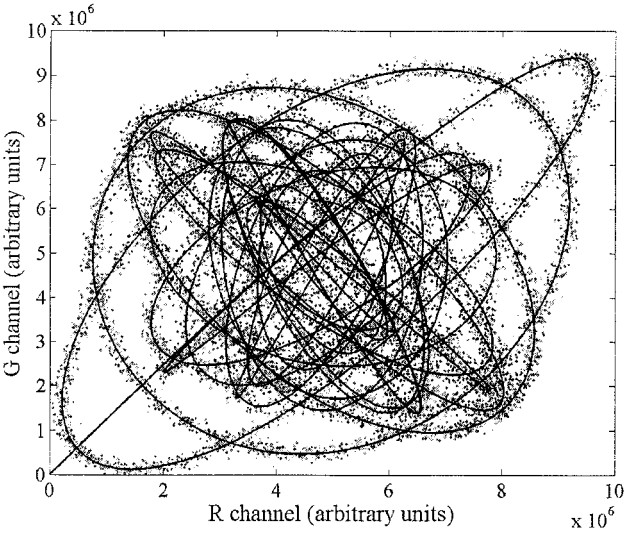

Fig. 3. RG projection of a simulated RGB LUT curve (solid curve) together with the RG values of a noisy Gaussian spatial retardation distribution (dots), both generated by means of Eqs. (1). It can be seen that the noise increases the width of the RG projection corresponding to the spatial distribution, which leads to greater errors for the standard RGB calibration algorithm.

Figure 4 shows the demodulation of the Gaussian-shaped retardation distribution used to generate Fig. 3. The plot shows a comparison of the profiles obtained by the standard RGB calibration algorithm, the modified method described, and the theoretical result. In this case the parameters used were $N = 420$, $M = 100$, $\beta = 1$, and an interpolation factor of 10; the size of the images was 400 pixels $\times$ 400 pixels with a maximum retardation value of 11.3 fringes. As can be seen, the results obtained by the improved RGB calibration method are much better that the

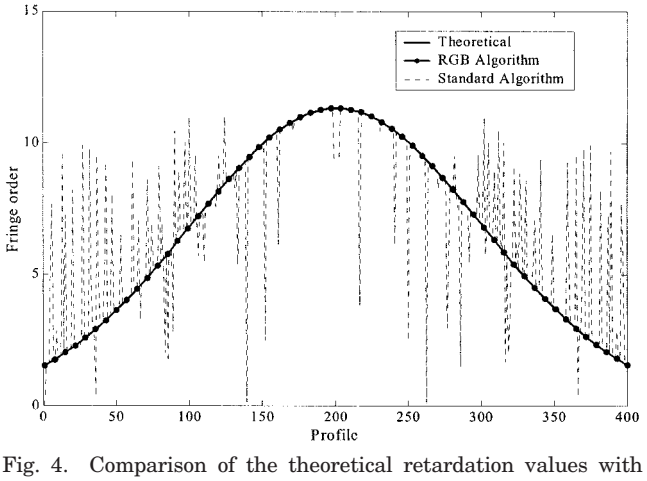

Fig. 4. Comparison of the theoretical retardation values with those obtained by the standard and improved RGB calibration algorithms. A significant reduction in the demodulation error can be observed when the improved algorithm is used.

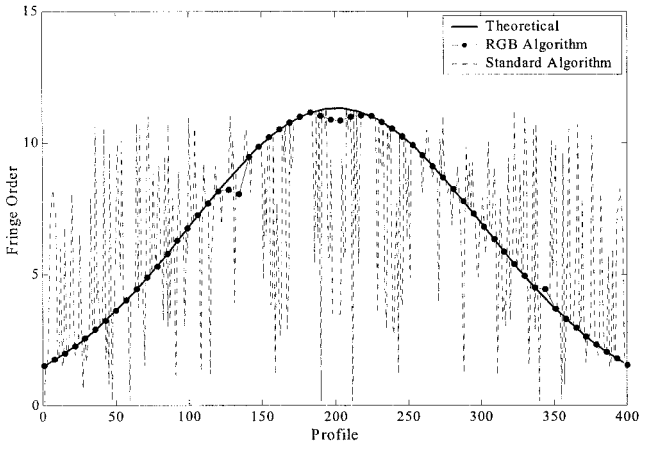

Fig. 5. Comparison of the theoretical retardation values with those obtained by the standard and improved calibration algorithms with chromatic coordinates rgb instead of RGB values. In this case the high values of the demodulation error obtained with the standard algorithm make it unreliable; however, the improved algorithm gives a good estimation of the retardation values.

standard technique. Figure 5 shows the same plot as in Fig. 4 but for rgb chromatic coordinates instead of the RGB values; in this case the noise level of the retardation recovered by the standard method makes it invalid. As we mentioned above, the use of chromatic coordinates, Eq (2), can have some advantages when the geometric conditions of the experiment change.

Although in this paper we have used the RGB LUT approximation for isochromatic demodulation, that is not the only possibility. Given the model of RGB formation as a function of the stress difference, one could minimize the error between the model and the observations as a function of the stress difference or, equivalently, the retardation Δ. In other words, if $F(\Delta)$ is the model function [for example, as given by Eqs. (1)], because there is spatial decoupling in the retardation, the objective will be to minimize $\tilde{U}(\mathbf{r}, \Delta) = [F(\Delta) - (R(\mathbf{r}), G(\mathbf{r}), B(\mathbf{r}))]^2$ as a function of Δ for each location $\mathbf{r}$. This approach, although the most appropriate from a statistical point of view, is not realistic in the particular case of photoelasticity for several reasons. First, the model given by Eqs. (1) is a simplification of the composition of RGB values; Terms corresponding to the quarter-wave dispersion, the dispersion of the photoelastic constant, and the possible misalignment of the elements of the polariscope have been not taken into account. Second, the spectral response of the RGB CCD camera is not easily obtainable. Third, the emission spectrum of the light source and the transmission spectra of the polariscope's elements, sample, and camera objective must be known. Finally the model for RGB formation as a function of the retardation will give rise to nonlinear equations, making the minimization difficult. For all of these reasons, the use of a experimentally obtained discrete estimation of $F(\Delta)$—the RGB LUT $[\hat{R}(\Delta_i), \hat{G}(\Delta_i), \hat{B}(\Delta_i)]$—combined with a regularization scheme and a selective search in the table, is a good solution, as we show in Section 3.

Because the proposed method is based on the measurement of the RGB LUT, the best setup will be the one that maximizes the modulation of the sinusoidal signals $R(\Delta)$, $G(\Delta)$, and $B(\Delta)$ (see Fig. 1); if the modulation is maximum, the distances between the different branches of the 3D RGB LUT (see Fig. 2) will be the greatest possible, thus minimizing the possibility of a mistake. Because we use commercially available photoelastic materials and CCD cameras, only the illumination spectrum remains as a free parameter. One can choose a great variety of illumination sources, such as lasers, filament lamps, discharge lamps, and fluorescent lamps. As is shown in Refs. 5 and 9 the best choice is a tricolour source, that is, a source whose spectrum is composed of only three wavelengths. These wavelengths must lie within the spectral regions defined by the three spectral responses of the RGB CCD. In the case of Yoneyama *et al.*[5] a special tricolour source is especially designed for this purpose. On the other hand, Quiroga and Gonzalez-Cano[9] show that a commercially available discrete-spectrum fluorescent lamp can also be used. Thus we have used the commercial type of illumination. Fluorescent lamps emit unpolarized light in such a way that the elements of the polariscope generate adequate states of polarization in a controlled way.

3. Experimental Results

We have tested the proposed RGB calibration method with real experimental data. The experimental setup consists of a circular polariscope, matched for the sodium line (λ_{Na} = 589 nm) and arranged in the circular dark-field configuration.[13] As a light source we used a discrete spectrum fluorescent lamp. The main advantage of using this kind of illumination instead of the conventional continuous spectrum light sources is an increment of the modulation for the RGB signals that makes it possible to demodulate the isochromatic phase correctly up to order 20. The photoelastic constant of the sample was 7000 (Pa m) fringe, and the thickness was 3.18 mm. The test object we used was an are-shaped sample under axial traction. We obtain the images in transmission mode with a three-sensor RGB CCD camera manufactured by JAI, Model M90.

Using this configuration, we measured the RGB LUT with an *f*-number of 5.5. This purpose we use a bar of the material described above with a width of 3.83 cm; we applied axial traction loaded from 0 to 100 kg in steps of 2.5 kg, so in this case $N = 40$. For every load a RGB subimage of 200 pixels $\times$ 200 pixels was obtained with the circular dark-field configuration of the polariscope. These images were obtained at the central part of the loaded bar, far from the clamping points; thus uniform stress differences within the image can be assumed. Afterward the mean R, G, and B gray levels are computed for each of the three channels of the image. The RGB LUT shown in Fig. 1 was obtained by our repeating this

procedure for each load. To express the stress difference pascals in instead of kilograms, it is necessary only to take into account that for the measurement conditions described above $\sigma_1 - \sigma_2 = L/(tw)$, where L is the load in kilograms, t is the thickness, and w the width of the bar. In Fig. 1 the three RGB values obtained for each load are plotted together; the points marked by symbols represent the experimental measurements, and the solid curve is the interpolation. Our objective in this procedure is to obtain an accurately measured RGB LUT; if the standard deviation of the gray levels of a single image is σ_{GV}, the standard deviation of the mean is $\sigma_m = \sigma_{GV}/\sqrt{Z}$, where Z is the number of samples. In our case, $\sigma_{GV} \approx 5$ gray levels; thus $\sigma_m = 0.03$ gray levels.

As mentioned above, in the RGB LUT method it is difficult to obtain a good model for the RGB formation; thus a quantitative discussion of the uncertainty in the stress difference implied by a given noise level as a function of position along the stress-parameterized locus in RGB space is not easy. For simplicity, let us assume monochromatic illumination and no error sources in the circular dark-field configuration of the polariscope; for these conditions we can always write

$$A(\mathrm{GV} - Z_0) = \cos(\Delta/\lambda), \tag{5}$$

where GV is the given gray-value image which can be any of the three channels R, G, or B; GV for a 8-bit system can vary between 0 and 255); A is the sensitivity, Z_0 the offset, Δ the retardation, and λ the wavelength of the monochromatic source. If $\sigma(\Delta/\lambda)$ and $\sigma(\mathrm{GV})$ are the uncertainties in Δ/λ and in the measured gray value, respectively, from Eq. (5) they are related by

$$\sigma\left(\frac{\Delta}{\lambda}\right) = \frac{1}{|\tan(\Delta/\lambda)|}\,\frac{\sigma(\mathrm{GV})}{|\mathrm{GV} - Z_0|}. \tag{6}$$

Although we have derived this expression for the simplest case, it reflects the basic behavior of the error of the recovered retardation: The bigger the gray value GV, the smaller the error of the retardation. Also, there is a cyclic dependence that is given by $|\tan(\Delta/\lambda)|$. For example, this cyclic dependence of $\sigma(\Delta/\lambda)$ is especially visible in Fig. 7 and 8 below, where chromatic coordinats r, g, and b are used.

Figure 6 shows a demodulation example; in this case the demodulation parameters were $M = 40$ and $\beta = 1$; the interpolation factor was 10, and the size of the images was 574 pixels $\times$ 768 pixels with a maximum retardation value of 4 fringes for λ_{Na}. Figure 6(a) shows the demodulated retardation obtained with the proposed method for the are-shaped sample. (To improve the figure we have superposed contour levels on the gray-scale image. Figure 6(b) shows the demodulation obtained by the standard RGB calibration method; in this case, the artifacts resulting from a bad demodulation are clearly visible. Finally, Fig. 6 (c) shows a comparison of the results

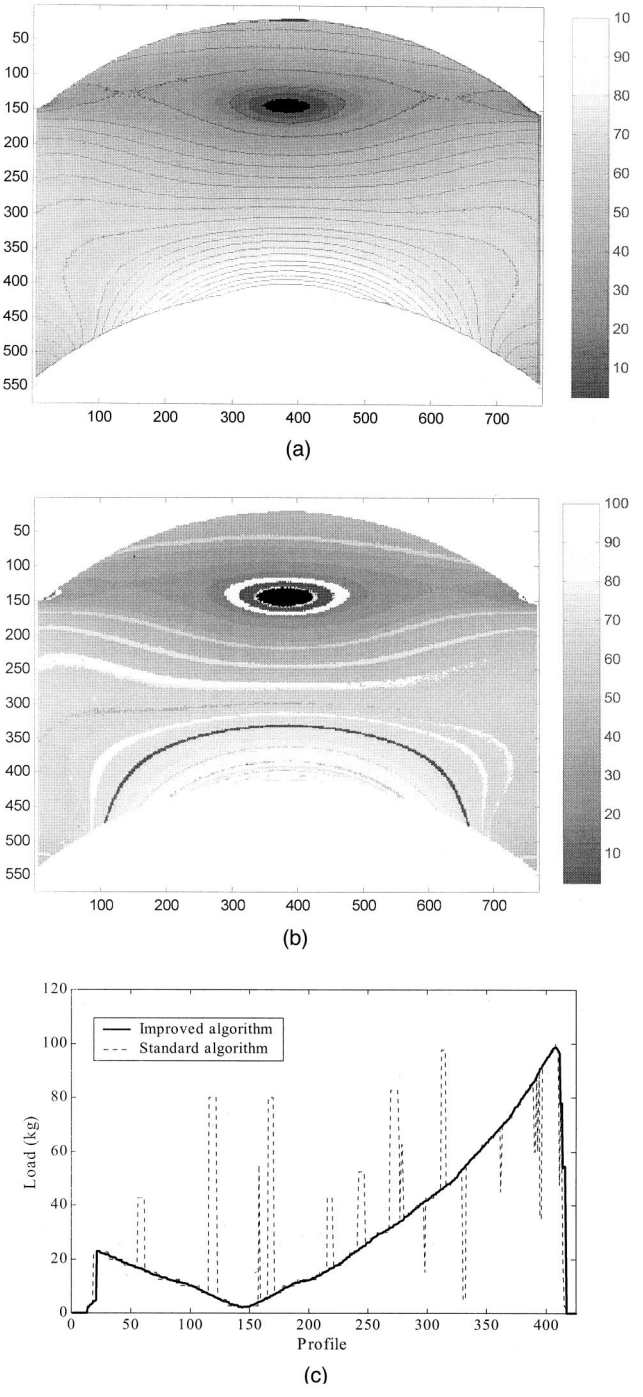

Fig. 6. (a) Retardation obtained for an arcshaped test object under axial traction. The demodulated retardation was calculated with the improved RGB calibration method proposed in this paper. Contour curves have been added for the sake of clarity (b) Distribution of the experimental values of the retardation obtained for an arc-shaped test object under axial traction. The demodulated retardation was calculated with the standard RGB calibration method. In this case, artiefacts that are due to bad demodulation are clearly seen. (c) Plot of the demodulated retardation along the central vertical profile of the object. Solid curve, results obtained with the improved algorithm; dashed curve, results of the standard algorithm.

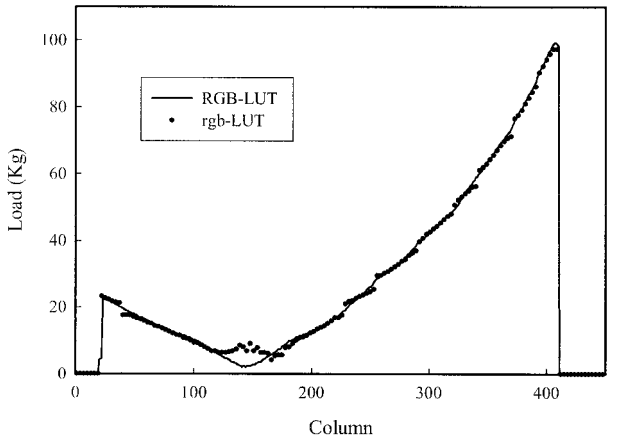

Fig. 7. Comparison of the demodulated retardation along the central vertical profile of the arcshaped object obtained with RGB values and chromatic coordinates *rgb* under the same geometric and chromatic conditions. Solid curve, results obtained with the RGB LUT; dotted curve, obtained with the rgb LUT.

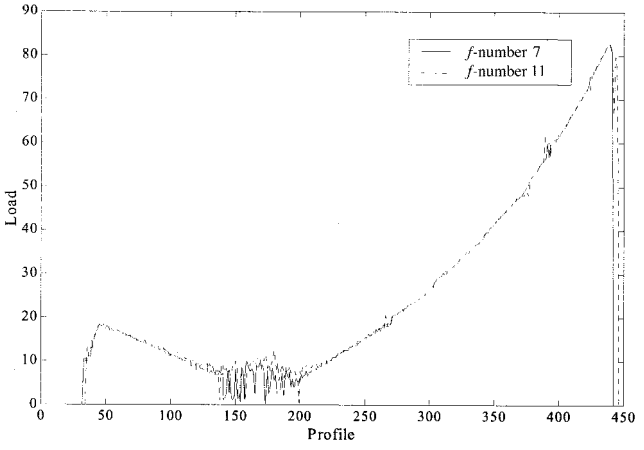

Fig. 8. Plot of the demodulated retardation along the central vertical profile of the test object for two different geometric conditions, in this case different *f*-numbers. In the two cases the rgb LUT was used, and it can be seen that the retardation values obtained are very close.

obtained by both methods for the central vertical profile.

As we have mentioned, if the geometric parameters change, the RGB LUT is no longer valid. This can be avoided by use of chromatic coordinates *rgb* instead of the obtained RGB values to yield a geometric-universal rgb LUT from a RGB LUT previously measured under given geometric conditions (*f*-number, distance to the sample, etc.). First we compared the results obtained by using both RGB LUT and rgb LUT methods to demodulate the retardation for the arc-shaped piece of Fig. 6. Figure 7 shows a plot with the demodulated phase obtained by both methods with the same demodulation parameters as in Fig. 6. To test the robustness of the rgb LUT algorithm against changes in the geometric parameters, we obtained two RGB isochromatic images for different apertures (*f*-numbers) of the CCD objective, in particular 7 and 11; we have demodulated the images by using rgb coordinates instead of RGB. Figure 8 shows a comparison, for the are-shaped sample of Fig. 6, of two vertical profiles along the same column obtained for the two mentioned apertures. As can be observed in Fig. 7 and 8, the result obtained is almost independent of the *f*-number used, but the rgb demodulation is noisier that the RGB, especially for low values of retardation (note the noise near the minimum region); this behavior arises because the error in the recovered rgb values increases when the RGB values are low, and in the circular dark-field configuration used these low RGB values are associated with low values for retardation. If the results are required to be independent of the geometric conditions, this error can be minimized if two different calibrations for dark and bright configurations of the circular polariscope are performed, but this will necessitate the acquisition of two images.

4. Conclusions

We have presented an improved RGB calibration technique for demodulation of the isochromatic phase from a single RGB image. The technique has proved to be robust and reliable even if chromatic coordinates *rgb* are used, which is an advantage if the results are required to be independent of the geometric conditions. The technique has been applied to isochromatic fringe patterns, but it can be applied to any problem of color image analysis in which a relationship between RGB values and the quantity to be measured can be previously determined.

Acknowledgments

We appreciate the financial support for this work given by the European Union project Advanced Integrated Nondestructive Testing Concepts for Unified Life-Cycle (INDUCE), BRPR-CT98-0805.

References

1. P. S. Theocaris and E. E. Gdoutos, *Matrix Methods in Photoelasticity* (Springer-Verlag, Berlin, 1979).
2. C. Buckberry and D. Towers, "Automatic analysis of isochromatic and isoclinic fringes in photoelasticity using phase-measuring techniques," Meas. Sci. Technol. **6,** 1227–1235 (1995).
3. Y. Morimoto, Y. Morimoto, and T. Hayashi, "Separation of isochromatics and isoclinics using Fourier transform," Exp. Tech. 1994; September/October 1994; pp. 13–17.
4. J. Carazo-Alvarez, S. J. Haake, and E. A. Patterson, "Completely automated photoelastic fringe analysis," Opt. Lasers Eng. **21,** 133–149 (1994).
5. S. Yoneyama, M. Shimizu, J. Gotoh, and M. Takashi, "Photoelastic analysis with a single tricolor image," Opt. Lasers Eng. **29,** 423–435 (1998).
6. A. Ajovalastic, S. Barone, and G. Petrucci, "Towards RGB photoelasticity: full-field automated photoelasticity in white light," Exp. Mech. September 1995, pp. 193–200.
7. J. A. Quiroga, and A. Garcia-Botella, "Demodulation of isochromatic RGB fringe patterns by a improved calibration technique," *Proceedings of the Fourth International Workshop on*

Automatic processing of Fringe Patterns, W. Osten and W. Jüptner, eds. Elsevier, Paris, (2001), pp. 126–133.
8. M. J. Ekman and A. D. Nurse, "Completely automated determination of two-dimensional photoelastic parameters using load stepping," Opt. Eng. **37,** 1845–1851 (1998).
9. J. A. Quiroga and A. Gonzalez-Cano, "Separation of isoclinics and isochromatics from photoelastic data using a regularized phase-tracking technique," Appl. Opt. **39,** 2931–2940 (2000).
10. J. A. Quiroga, M. Servin, and J. L. Marroquin, "Regularized phase tracking technique for demodulation of isochromatics from a single tricolour image," Meas. Sci. Tech. **13,** 132–140 (2002).
11. W. Liu, Z. Wang, G. Mu, and Z. Fang, "Color-coded projection grating method for shape measurement with a single exposure," Appl. Opt. **39,** 3504–3508 (2000).
12. M. Hartl, I. Krupka, and M. Liska, "Diferential colorimetry: tool for evaluation of chromatic interference patterns," Opt. Eng. **36,** 2384–2391 (1997).
13. K. Ramesh, *Digital Photoelasticity* (Springer-Verlag, Berlin, 2000).